Probing the hidden magmatic evolution of El Misti volcano (Peru) with the Pb isotope composition of fumaroles

Ivan Vlastélic, Fredy Apaza, Pablo Masias, Marco Rivera, Jean-Luc Piro, Abdelmouhcine Gannoun

Probing the hidden magmatic evolution of El Misti volcano (Peru) with the Pb isotope composition of fumaroles

Ivan Vlastelic[1*], Fredy Apaza[2], Pablo Masias[2], Marco Rivera[3], Jean-Luc Piro[1], Abdelmouhcine Gannoun[1]

[1] Université Clermont Auvergne, CNRS, IRD, OPGC, Laboratoire Magmas et Volcans, F-63000 Clermont-Ferrand, France

[2] Instituto Geológico Minero y Metalúrgico (INGEMMET), Arequipa, Peru

[3] Instituto Geofísico del Perú, Observatorio Vulcanológico del Sur, Mz B, Lt 19, Urb. La Marina, Cayma, Arequipa, Peru

* Corresponding author

email address: ivan.vlastelic@uca.fr

Phone : + 33 4 73 34 67 10

ORCID ID : 0000-0002-6701-4832

Abstract

This work proposes a new method to probe the hidden magmatic evolution of quiescent Andean volcanoes from the Pb isotope composition of gases. The method is based on an Assimilation-Fractional Crystallization-Degassing model linking the Pb isotope composition of gases with the SiO_2 content of their magmatic source. The model is applied to El Misti volcano that threatens Arequipa, the second most densely populated city of Peru.

Gas condensates and Pb-rich solid deposits (PbS, $PbCl_2$, $PbSO_4$) collected in 2018 in the bottom of El Misti crater at 260 - 150°C fumaroles vents were used to reconstruct the mean composition of degassing magmas (60.8-61.8 wt.% SiO_2). These compositions are slightly more evolved than the lavas from the last AD 1440–1470 eruption, suggesting either the secular differentiation of the main magma reservoir, or the contribution of more evolved magmas to volcanic gases. On the other hand, the slight but significant difference between the instantaneous composition recorded in gas condensates and the time-integrated composition recorded in solid deposits points to the degassing of less evolved magmas over the last decades. This trend is ascribed to a recent recharge of El Misti reservoir with hot mafic magmas, in agreement with the evolution of fumarolic deposit mineralogy in the last half a century. The Pb isotope composition of gas appears to be a promising tool for probing the hidden magmatic evolution of quiescent volcanoes where Assimilation-Fractional Crystallization operates.

Keywords: El Misti volcano, Assimilation-Fractional Crystallization, magmatic gases, fumaroles, sublimates, Pb isotopes

Acknowledgments:

We thank two anonymous reviewers for their constructive comments and William W Chadwick for handling the manuscript. IV acknowledges OVI personnel for their welcome in Arequipa. This research was financed by the Institut de Recherche pour le Développement, the French Government Laboratory of Excellence initiative n° ANR-10-LABX-0006, the Region Auvergne and the European Regional Development Fund. This is Laboratory of Excellence ClerVolc contribution number XXX.

Introduction

El Misti stratovolcano threatens the city of Arequipa, the second most densely populated city of Peru (>1.1 million inhabitants, INEI, 2018) that is continuously growing at its foot (Fig. 1). Over the last 50 000 years the volcano has shown a cyclic activity, with Plinian eruptions every 2000 to 4000 years and smaller to moderate explosive eruptions every 500 to 1500 years, on average (Thouret et al., 2001). The lavas produced since 0.12Ma are andesitic to dacitic in composition, with rare rhyolites and no marked evolution through time (Rivera et al., 2017). This relative homogeneity contrasts with the mineral evidence for regular recharge and mixing, which led Ruprecht and Wörner (2007) to suggest that magma recharge events are more frequent in comparison to the eruption frequencies, and that El Misti reservoir evolves most of the time cryptically. Since the last major eruption (A.D. 1440–1470), El Misti crater has showed a persistent but fluctuating degassing activity (Thouret et al., 2001; Moussallam et al., 2017). Over the last decades, the temperature of gases has varied between 125°C and 310°C (Hantke and Parodi 1966; Birnie and Hall, 1974; Thouret et al. 2001, and observations from Observatorio Vulcanológico del Ingemmet (OVI) and Instituto Geofísico del Perú (IGP)). The gases sampled in 2015 showed a dominant magmatic signature with little evidence for interaction with rocks and hydrothermal fluids (Moussallam et al, 2017), which contrasts with the dominance in 1967 of low-temperature minerals formed by gas-rock interactions (Birnie and Hall, 1974). Moussallam et al. (2017) acknowledged that the current composition of the magmatic source is unknown, and may be similar to either the rhyolitic or andesitic magmas that interacted during the c. 2030 - 2000 years B.P. eruption (Thouret et al., 2001; Cobeñas et al., 2012; Harpel et al., 2011). In the absence of direct measurement, the estimation of the current state and evolution of the El Misti magma reservoir is challenging but important.

This study aims to reconstruct the composition of the El Misti magmatic reservoir from the Pb isotopic composition of gas emitted in the summit crater. Lead isotopes are well suited for this purpose because (1) lead is a volatile metal enriched in El Misti gases and fumarolic deposits (Birnie and Hall, 1974), (2) the heavy Pb isotopes (^{208}Pb, ^{207}Pb, ^{206}Pb and ^{204}Pb) do not fractionate measurably during magma degassing, due to their very small relative mass differences (Vlastelic et al., 2013), so that the Pb isotopic composition of gas reliably records that of the degassing magma source, (3) the Pb isotopic composition of magma is tightly related to the degree of magma differentiation through the Assimilation - Fractional

Crystallization (AFC) process that dominates the compositional evolution of El Misti magmas (Mamani et al., 2008; Kiebala, 2008; Rivera et al., 2017). Lead isotopes are especially sensitive to AFC as mantle melts and crustal basement display highly contrasted Pb contents and isotopic compositions (Tilton and Barreiro, 1980; Barreiro and Clark, 1984). We have applied this approach to gas condensates and fumaroles deposits sampled in the bottom of El Misti crater in October 2018.

Geological setting

El Misti volcano (5822 m above sea level) is located to the north of the Andean Central Volcanic Zone (CVZ) at 16°16′ S and 71°22′ W (Fig. 1a). It sits on the western flank of the Western Cordillera, about 240 km east of the Peru-Chile trench. A detailed description of El Misti's evolution is given in Thouret et al. (2001) and Rivera et al. (2017). Briefly, the composite edifice comprises an older main stratovolcano (Misti 1, ca. 833–112 ka), on which grew three younger strato-cones (Misti 2, 3 and 4). Large volumes (4 – 6.5 km^3) of dacitic pyroclastic density currents (PDC) were emplaced between c. 50 000 and 40 000 and again between c. 13 700 and 11 300 years B.P., the last of which resulted in the formation of today's summit crater. The most recent Plinian eruption (c. 2030 – 2000 years B.P.) produced 1.4 km^3 of pumice-fall deposits that spread ≥25 km from the vent and 0.01 km^3 of PDC deposits (Harpel et al., 2011). The mingling texture of rhyolitic and less evolved andesitic components in the pumices were ascribed to the injection of an andesitic magma from 7-12 km depth into a shallower rhyolitic reservoir (Tepley et al., 2013). This major event is most likely responsible for the formation of today's 900 m-wide summit crater. The last major eruption (AD 1440–1470, VEI 2) produced andesitic ash-fallout and led to the formation of a lava dome inside the present-day inner crater. Since then, the El Misti crater has shown a persistent degassing activity, with periods of increased fumarolic emissions and possible phreatic events in 1667, 1784-1787 and 1949 (Bullard, 1962; Chavéz Chavéz, 1992; Thouret et al., 2001). Less than 12 km separate El Misti crater from the nearest Arequipa suburbs (Fig. 1b).

Samples and methods

We carried out field work in the El Misti crater in October 2018, at the end of the dry season. After a survey of the lava dome, gas condensates and sublimates were collected at the hottest fumarole vent (Fig. 1c) where a temperature of 260°C was measured using a Fluke 62 Max infrared thermometer. Gas condensates were collected in a savillex teflon elbow emplaced in the vent. Gas sublimates were subsequently sampled 30 cm underground at the lower surface of a lava block that obstructed the vent. Sub-surface sublimates were also collected at another vent with a temperature of 150°C (Fig. 1c). Samples were chemically treated and analysed at Laboratoire Magmas et Volcans (LMV) in France. The sublimates were investigated by Scanning Electron Microscopy (SEM, JSM 5910LV) operating in Backscattered Electron (BSE) imaging mode. Sublimate mineralogy was determined from qualitative analyses of major elements using Energy Dispersive Spectrometry (EDS). All chemical treatment of the samples was done in LMV's clean room, within hoods equipped with HEPA filters, and using savillex teflon vials and highly pure acids. One millilitre of the gas condensate was gently evaporated at 60°C and re-dissolved in 1 ml of 0.5M HNO_3 - 0.05M HF. Representative chips of the sublimates (0.2 to 100 mg in size) were fully dissolved in 6N HCl at 80°C. The condensate and sublimate solutions were aliquoted for the analysis of trace element abundance and Pb isotope composition.

Prior to ICPMS analysis, the sublimate aliquots were evaporated and re-dissolved in 0.5M HNO_3 - 0.05M HF, to reach dilution factors of 10^5 (solution/sublimate mass ratio). All volumes were precisely weighted with a precision better than 10^{-4}g. The trace element abundances were determined by quadrupole ICPMS (Agilent 7500), in plasma robust mode (1550 W), using the reaction cell (He mode) to reduce interferences on masses ranging from 45 (Sc) to 77 (Se). The signal was calibrated externally (every 4 samples) with a synthetic standard (Inorganic Venture). The acid media was also measured every 4 samples to correct for background signal. Repeated analysis of the analysed solutions yielded 2σ errors of < 5% for Ti, V, Cr, Mn, Co, Ni, Cu, Rb, Sr, Zr, Nb, Sn, Ba, Pb and < 8 % for As, Cd, In, Sb, Tl and Bi.

Lead was separated using Eichrom Sr specific resin following the method of Deniel and Pin (2001). Procedural blanks were < 0.03 ng for Pb, which is insignificant compared to the amounts of Pb extracted from samples. Lead isotope compositions were measured on a Thermo Fisher Scientific Neptune Plus MC-ICPMS. Purified Pb was dissolved in 0.05M HNO_3 in order to obtain 150 ppb Pb solutions. The sample solutions were introduced in the mass spectrometer using a 100 μL/min nebulizer coupled to a quartz cyclonic spray chamber,

yielding a total Pb signal between 18 and 20 volts. The Pb instrumental mass fractionation was corrected during measurement by doping the Pb solutions with the Thallium (Tl) NBS997 standard, applying a Pb/Tl ratio of 5. The NBS981 Pb standard was measured between every two samples to correct Pb ratios for instrumental drift and the slight difference in mass fractionation between Pb and Tl. Data were normalized to the NBS981 standard using the values of Todt et al. (1996). Repeated analysis of the NBS981 standard every two samples yielded intra-session 2σ reproducibility better than 100, 120 and 140 ppm for $^{206}Pb/^{204}Pb$, $^{207}Pb/^{204}Pb$ and $^{208}Pb/^{204}Pb$, respectively.

Results

The chemical and isotopic composition of the 2018 El Misti condensates and sublimates are reported in Table 1. Images of the sublimates are shown in Fig. 2, and trace element contents are plotted in Fig. 3. The 260°C gas condensate contains 177 ppb Pb, 37-38 ppb of Tl and Zn, and 9-12 ppb of Bi, Cu, and Sb, with the latter concentrations being at the low range of volcanic gases (Zelenski et al., 2021). The condensate also contains significant amounts of refractory elements (244 ppb Ba, 45-46 ppb of Sr and Ti). The 260°C gas sublimates occur as a foam of anhydrous alum ($NaAl(SO_4)_2$), several millimetres in thickness, and coated in many places with galena (PbS) (Fig. 2). The five representative chips analysed for bulk composition contain 2 - 10 wt. % Pb, 0.4 – 1 wt. % Ti, 4100 - 9500 ppm Tl, 5400 - 9400 ppm Zn, 2200 - 4600 ppm Bi, 2100 - 3600 ppm Cd, and 600 - 3200 ppm Sn. The 150°C gas sublimates occur as thin patches of anglesite ($PbSO_4$) and cotunnite ($PbCl_2$), with minor anhydrite ($CaSO_4$), coating the lower surface of a lava block (Fig. 2). The light yellow cotunnite and shiny black anglesite are barely visible without the use of optical aids. The bulk analysis of four separates yielded 16.8 - 44.5 wt.% Pb, 142 - 1349 ppm Tl, 399 - 1689 ppm Zn, 81 - 114 ppm Bi, and 539 - 2257 ppm Cd. The $^{206}Pb/^{204}Pb$, $^{207}Pb/^{204}Pb$ and $^{208}Pb/^{204}Pb$ ratios of the 260°C gas condensate are 17.724 ± 0.003, 15.592 ± 0.004, and 38.628 ± 0.005, respectively. The 260°C and 150°C gas sublimates display significantly less radiogenic, but very homogeneous Pb isotope composition, with average $^{206}Pb/^{204}Pb$, $^{207}Pb/^{204}Pb$ and $^{208}Pb/^{204}Pb$ ratios of 17.676 ± 0.002, 15.584 ± 0.004, and 38.598 ± 0.014, respectively. These ratios are within the ranges of previously analysed El Misti rocks (Mamani et al., 2008).

The composition of the gas condensates and sublimates collected in 2018 show marked differences when compared to those collected in July 1967 by Birnie and Hall (1974) (Fig. 3) while the temperature of the fumaroles was only 100-125°C: (1) The Zn concentration of the 2018 gas condensate (37 ppb) is an order of magnitude lower than in the 1967 condensates (240-740 ppb Zn); (2) The 2018 sulfates are dominantly Na-Al sulfate instead of Ca sulfates in 1967 (anhydrite and gypsum) in agreement with the hotter temperature of the 2018 gases. This difference in sulfate mineralogy is recorded by Sr, which is much lower in 2018 sulfates (Fig. 3); (3) Pb-rich phases such as galena, cotunnite, and anglesite are common in 2018, whereas they were not detected in 1967 samples. Consequently, the 2018 Na-Al sulfates are enriched in Pb and Tl compared with the 1967 anhydrite and gypsum with less than 2400 ppm Tl and 8300 ppm Pb.

Origin of the Pb isotopic composition of fumaroles samples

The Pb isotopic composition of fumarolic samples potentially records several processes, such entrainment of rock particulates, mixing between magmatic and hydrothermal gases, and variations of the magmatic source composition. The contribution of rock particulates to the Pb content of gas samples is assessed using the enrichment factor of Pb (Eq. 1):

$$EF_{Pb} = (Pb/X)_{gas\ samples}/(Pb/X)_{lava}$$

where X is a refractory rock-derived element (Symonds et al., 1987). Using titanium as rock-derived element, and the average composition of the lavas from "Misti 4" (12.3 ppm Pb and 5050 ppm Ti; Rivera et al., 2017), EF_{Pb} is 1.6 x 10^3 in the condensate, 0.8 – 9.4 x 10^3 in the 260°C sublimates, and 0.8 – 4.4 x 10^5 in the 150°C sublimates. The lead fraction unsupported by silicate input ($1 - 1/EF_{Pb}$) is 99.94 % in the condensate, >99.87 % in the 260°C sublimates and >99.999 % in the 150°C sublimates (Fig. 4). Repeating this calculation with other rock-derived elements, such as Zr, Nb or Y, and "Misti 4" end-member rock compositions, yields in all cases more than 99.7 % Pb unsupported by silicate input, confirming that the contribution of rock particulates is extremely small. This tiny contribution does not account for the small isotopic variations in gas condensates and sublimates, which do not correlate with EF_{Pb} (Fig. 4). The dry composition (H_2O/SO_2 molar ratio of 32 ± 3) of El Misti gases also only requires

a minimal contribution of the hydrothermal system (Moussallam et al., 2017). The contribution of low temperature hydrothermal vapours does not seem to affect the Pb isotope signature of the sublimates, which does not vary with vent temperature. The remaining and most likely possibility is that Pb isotope ratios of the fumarolic samples reflect the composition of magmatic gases.

Assimilation-Fractional Crystallization-Degassing model

The Pb isotopes of magmatic gases can be linked to the degree of crystallization of their magmatic source through an Assimilation-Fractional Crystallization-Degassing (AFCD) model. This model takes advantage of the properties of heavy Pb isotopes which do not fractionate during magma degassing, allowing us to reconstruct the Pb isotope composition of magmas from gas composition. Then, we infer the degree of magma crystallization from the Pb isotope composition of magmas using an Assimilation-Fractional Crystallization model. The two steps and related assumptions of the AFCD model are described below, and solutions for one and two magma reservoirs are provided.

Degassing

Lead is a moderately volatile element in magmatic systems, with a coefficient of emanation (i.e., fraction of Pb outgassed) in the range of 1-2% (Gauthier et al., 2000). Lead volatilizes dominantly as chloride and condenses mostly below 500°C (Symonds et al., 1987). The Pb isotope compositions of gas is related to that of the degassing magma by the coefficient of isotopic fractionation α (Eq. 2) :

$$(^{206}Pb/^{204}Pb)_{gas} = \alpha_{64} (^{206}Pb/^{204}Pb)_{magma}$$

in the case of the $^{206}Pb/^{204}Pb$ ratio. The theoretical kinetic isotope fractionation ($\alpha_{kin} = (m_{204}/m_{206})^{0.5} = 0.995$) represents an extreme value of α_{64}, which is closer to unity in natural systems due to back condensation reactions at the gas - magma interface (Richter, 2004). Practically, isotopic fractionation of Pb during magma degassing is smaller than the precision of Pb isotope measurements (Vlastelic et al., 2013), and is not significant compared to the

variations occurring in lavas. In such situations, α must be very close to unity for all Pb isotope ratios, and the Pb isotope compositions of the fumarole samples must reliably reflect that of the degassing magma. In the case of simultaneous degassing of andesite and rhyolite magma reservoirs, the composition of the gas mixture is obtained by mass balance (Eq. 3):

$$(^{206}Pb/^{204}Pb)_{gas} = \Phi_{andesite} \times (^{206}Pb/^{204}Pb)_{andesite} + \Phi_{rhyolite} \times (^{206}Pb/^{204}Pb)_{rhyolite}$$

with $\Phi_{andesite} + \Phi_{rhyolite} = 1$

where Φ is the fraction of the total Pb gas flux, which depends on the size and degassing rate of each reservoir.

Assimilation-Fractional Crystallization

Mantle derived magmas ascending through continental arcs tend to melt and assimilate crustal rocks with low melting temperature. Because wall-rock assimilation consumes heat, while crystallization releases heat, the two processes are potentially coupled. However, the ratio of assimilation to crystallization rate (referred to as r) largely varies in magmatic systems, generally between 0.2 and 2.7. These variations depend on several parameters including the initial temperature and melting point of the country rock, and the thermal potential of the parental magma (Thompson et al., 2002). For instance, r is typically in the range of 1.0-1.5 for an initial magma temperature of 1350-1150°C, compared to 0.6-0.2 for a temperature of 1150-900°C. The efficiency of assimilation is predicted to decrease (1) during differentiation due to the decreasing liquidus temperature, and (2) with decreasing depth as the temperature of host rocks decreases following the geothermal gradient. Both trends suggest that assimilation takes places most pronouncedly during earlier, deeper magmatic stages.

A major outcome of AFC is that the isotopic variations of continental arc lavas often correlate with the degree of differentiation (De Paolo, 1981). The isotopic record of AFC is particularly clear along the CVZ where Pb isotope variations are controlled by the assimilation of Pb-rich rocks from the locally thick continental basement (e.g., Tilton and Barreiro, 1980; Wörner et al., 1992; Mamani et al. 2008; Kiebala, 2008; Sainlot et al., 2020a). At El Misti, the Assimilation-Fractional Crystallization process translates in a decrease of $^{206}Pb/^{204}Pb$, $^{207}Pb/^{204}Pb$ and

283 $^{208}Pb/^{204}Pb$ with increasing SiO_2, due to assimilation of the proterozoic Charcani gneiss
284 (Arequipa Massif) of the Western Cordillera basement with unradiogenic Pb ratios
285 ($16.792<^{206}Pb/^{204}Pb< 17.088$) (Tilton and Barreiro, 1980; Barreiro and Clark, 1984; Mamani et
286 al., 2008; Kiebala, 2008). Tilton and Barreiro (1980) pointed out that the granulitic gneiss must
287 have a lower crustal origin, but is probably assimilated by El Misti lavas at shallower depth.
288 We hypothesize that the frequent passages of magma in the lower crust favour the
289 disaggregation of crustal rocks into small xenoliths (Thompson et al., 2002). Entrained
290 xenoliths could partially dissolve during magma ascent in the upper crust due to superheating
291 above the liquidus (Brearley and Scarfe, 1986). How and where El Misti magmas are
292 contaminated remains uncertain, but contamination must be related to magma
293 crystallization, which dominantly occurs between 7 and 12 km depth (Tepley et al., 2013).
294 The AFC relation might have substantially varied during the growth of El Misti volcano due to
295 slight variations in magma path and thermal history, in particular following major collapses,
296 and heterogeneity of the basement. For this reason, we use the AFC relation defined over the
297 most recent Misti 4 stage (<11 ky) (Fig. 5), assuming that the composition of mantle derived
298 magmas and assimilated rocks, as well as the r value, do not vary at short time scales. This
299 relation is defined based on four samples analysed for Pb isotopes by Mamani et al. (2008),
300 including 6 ka old scoria from pyroclastic density current deposits (MIS-00-20), two pumices
301 from fall deposits (quebrada San Lazaro) and one pumice (MIS-02-10a) from the 2030-2000
302 years B.P. eruption. The SiO_2 contents of these samples, between 58.7 and 63.2 wt.%,
303 encompass the range of variations of El Misti rocks with the exception of rhyolites. The
304 samples show a Pb isotope range ($17.3965<^{206}Pb/^{204}Pb<17.8442$) that brackets the
305 composition of the fumarole samples ($17.6740<^{206}Pb/^{204}Pb<17.7243$), and are thus
306 appropriate for calibrating the AFC relationship. In addition, these samples do not contain
307 large minerals, with potential Pb isotope disequilibria relative to the matrix, so it can
308 reasonably be assumed that their bulk composition reflects that of the degassing melt. The
309 black ash fall sample (MIS-02-06), with a proposed age of 11 ky (Kiebala, 2008) is not included
310 because (1) this sample pertains to Misti 3 (Rivera et al., 2017), and (2) the juvenile origin of
311 the ashes is uncertain. For the purpose of modelling, we preferentially use the $^{206}Pb/^{204}Pb$ and
312 $^{208}Pb/^{206}Pb$ ratios, which show well-defined AFC trajectories owing to large variations in lavas
313 and precise measurements. The $^{207}Pb/^{204}Pb$ and $^{208}Pb/^{204}Pb$ ratios, with smaller variations and

larger errors are not used. The relationships between SiO_2 content and Pb isotope ratios in lavas from Misti 4 stage are best fitted (R^2> 0.988) by the second-degree polynomial functions:

$$SiO_2\ (wt\%)_{magma} = -26.015 \times (^{206}Pb/^{204}Pb)_{magma}^2 + 906.56 \times (^{206}Pb/^{204}Pb)_{magma} - 7834.7 \quad \text{(Eq. 4)}$$

$$SiO_2\ (wt\%)_{magma} = -3163.95 \times (^{208}Pb/^{206}Pb)_{magma}^2 + 13949.16 \times (^{208}Pb/^{206}Pb)_{magma} - 15311.5 \quad \text{(Eq. 5)}$$

These relations defined over a SiO_2 range of 58.7- 63.2 wt.% probably do not hold for rhyolites for two reasons: (1) if the final crystallisation of rhyolites occurs mostly within the volcanic edifice (~3 km depth), as suggested by Tepley et al. (2013), it is expected that rhyolites assimilate older Misti rocks and not the Charcani gneiss (Arequipa Massif). In keeping with this idea, Barreiro and Clark (1984) noted that the most contaminated El Misti rhyolite has a $^{206}Pb/^{204}Pb$ ratio of 17.38, barely lower than the dacitic pumice sample MIS-02-10a (17.3965). (2) Crustal assimilation markedly decreases during late stage crystallisation (Thompson et al., 2002). Thus, the Pb isotope composition of gases is probably less sensitive to late stage crystallisation of magmas at shallow depth, which may constitute the main limitation of the model.

Reconstructed mean composition of degassing magmas

The model provides, as a general solution, the mean composition of degassing magmas. The mean composition does not constrain the composition and distribution of heterogeneities (i.e. multiple magma reservoirs) within the system. The mean composition of degassing magmas can be reconstructed by combining degassing (Eg. 2) and AFC equations (Eqs. 4 and 5). From Eqs. 2 and 4, we estimate the SiO_2 content of degassing magmas at 60.81 wt.% for the gas condensate and at 61.50 wt% for the average of the gas sublimates. Using Eq. 5 based on the $^{208}Pb/^{206}Pb$ ratio instead of Eq. 4 gives slightly higher SiO_2 concentrations of 61.19 wt.% and 61.81 wt%, respectively. In both cases, the gas sublimates record a more evolved composition (+0.62 to +0.69 wt.% higher SiO_2) compared to the gas condensate. The 100 ppm analytical uncertainty on the Pb isotope ratios of the fumaroles samples (Table 1) translates into a relative uncertainty of less than 0.03 wt.% on the estimated SiO_2 values. The absolute error

on the SiO_2 estimates still remains controlled by the precision of the SiO_2 concentration data used in Eq. 4-5, which does not exceed 0.3 wt.%. In Fig. 6, the estimated SiO_2 concentrations of the degassing magmas are compared to the long-term evolution of the SiO_2 content of El Misti lavas. The results of the model can be directly used to trace the evolution through time of a single large magma reservoir (Fig. 6a).

Degassing of two reservoirs of known composition

In the model of Tepley et al. (2013), an additional smaller rhyolitic magma reservoir transiently forms in the shallow crust (ca. 3km) every 2000 to 4000 years. It is not known whether such a rhyolite reservoir has existed since the last 2030-2000 years B.P. Plinian eruption. If it exists, one can envision that both deep andesite and shallow rhyolite magmas contribute to the gases escaping from El Misti crater. In this case, specific model solutions can be obtained considering that the Pb flux from each reservoir (Φ) might also contribute to the Pb isotope composition of the gas mixture at the surface according to Eq. 3, in addition to the contrasted compositions of the magma sources. In an end-member situation, the compositions of the magma reservoirs are constant and the composition of the gas is entirely controlled by varying Φ (Fig. 6b). The model then allows the relative contributions of two reservoirs of known composition to be quantified. The $^{206}Pb/^{204}Pb$ ratio of the andesite reservoir can be assumed to be the same as the least evolved scoria MIS-00-20 (17.8442). In the absence of published Pb data on rhyolites, the Pb composition of the rhyolite reservoir can be assumed to be the same as the dacitic pumice MIS-02-10a ($^{206}Pb/^{204}Pb$ =17.3965) because, as argued above, late-stage differentiation of magmas within the edifice probably does not markedly modify Pb isotope composition. With these compositions, solving Eq. 3 yields $\Phi_{andesite}$=73% and $\Phi_{rhyolite}$=27% for the gas condensate, and $\Phi_{andesite}$=62% and $\Phi_{rhyolite}$=38% for the gas sublimates. In this model, the contribution of gaseous Pb from the rhyolite reservoir is about 10% higher in gas sublimates than in gas condensates.

Hidden evolution of the El Misti magma reservoir

Evolution since the last eruption (AD 1440–1470)

The modelled composition (60.81- 61.81 wt.% SiO_2) of magmas currently degassing at El Misti volcano is similar to the average composition of El Misti magmas (61.0 ± 3 wt.% SiO_2, n= 116, Rivera et al., 2017). The model results preclude highly evolved magmas, such as those sampled during the last Plinian eruption with >63 wt.% SiO_2 (Thouret et al., 2001; Tepley et al., 2013), being the dominant source of the 2018 gases. Yet, the modelled 2018 composition is slightly more evolved than that of the most recent lavas, in particular those forming the conduit plug with a SiO_2 content generally below 58.9 wt.% (Rivera et al., 2017) (Fig. 6). There are two possible interpretations of this shift depending on the interpretation chosen for the structure of the El Misti plumbing system. In the hypothesis of a single, large magma reservoir undergoing cycles of recharge and differentiation (Ruprecht and Wörner, 2007), the SiO_2 increase inferred here from Pb isotopes indicates that magma differentiation has been on average more important than magma recharge over the last few centuries (Fig. 6a). On the other hand, in the two-reservoir model of Tepley et al. (2013), one can assume that the andesite and rhyolite magmas preserve more or less constant compositions at the secular scale (Fig. 6b). The evolved composition of currently degassing magmas (relative to the lavas from the last eruption) can be explained by the contribution of gases from the shallow rhyolitic magmas to the main gas flux.

Current evolution

The small Pb isotope difference between gas sublimates and gas condensate cannot reflect the simultaneous input of different gases at the same vent. Instead, this difference can be related to the fact that the condensate provides an instantaneous composition (at the time of sampling in October 2018) whereas the solid deposit records a composition averaged over the time of formation of the deposit. This time must be less than 48 years because the Na-Al sulfates and the Pb-rich minerals were not already formed in July 1967 (Birnie and Hall, 1974). The difference between the instantaneous (60.81- 61.19 wt.% SiO_2) and time-integrated (61.50- 61.81 wt.% SiO_2) SiO_2 estimates thus records the degassing of less evolved magma through time. A straightforward implication from the single magma reservoir hypothesis is that the magmatic reservoir is currently undergoing recharge by hot mafic magmas (Fig. 6a). In the two-reservoir model of Tepley et al. (2013), the current evolution of gas composition

409 could instead reflect the decreasing contribution of gases from the shallow rhyolitic reservoir,
410 possibility due to its progressive solidification (Fig. 6b).
411 The recharge hypothesis is independently supported by the mineralogy of the gas sublimates.
412 The Pb minerals (PbS, $PbSO_4$ and $PbCl_2$) occurring in the El Misti 2018 fumaroles deposits are
413 typically formed by the condensation of high-temperature magmatic gas (Symonds et al.,
414 1987; Taran et al., 2000; Africano et al., 2002). These gases can be similar to those sampled in
415 2015, with an equilibrium temperature of 532 °C and fO_2 equivalent to ΔQFM = +2.8
416 (Moussallam et al., 2017). In these conditions, galena forms first and is replaced by cotunnite
417 and anglesite as the temperature decreases and fO_2 increases. At El Misti, the occurrence of
418 $PbSO_4$ and $PbCl_2$ below 300°C requires little or no mixing of magmatic gas with air (Africano et
419 al., 2002). The occurrence of galena at the 260°C vent and cotunnite-anglesite at the 150°C
420 vent is thus consistent with closed-system condensation of the same high-temperature
421 parental gas that probably feeds the whole fumarolic field. The 2018 mineral assemblage
422 contrasts with the 1947 low temperature mineral suite (sulfur, anhydrite, gypsum and
423 ralstonite) that results from extensive gas rock interaction (Birnie and Hall, 1974). Part of this
424 difference might reflect sampling bias because Birnie and Hall (1974) did not sample
425 underground deposits whereas we did not sample sulfur and other minerals from low
426 temperature vents. However, the absence of high-temperature minerals in all five samples
427 collected in 1967 suggests overall colder degassing conditions in agreement with the lower
428 measured temperature (100-125°C). Fumarole deposits grow very slowly, on the order of
429 μm/day (Johnson and Burnett, 1993; Sainlot et al., 2020b) and average out short-term
430 fluctuations of degassing conditions. The difference in mineral assemblage between 1967 and
431 2018 is a robust observation that indicates a recent increase in gas temperature. The
432 important increase of gases temperature (>100°C) cannot reflect a comparable increase of
433 magma temperature but might reflect both a shallower and slightly hotter magma source, and
434 overall conditions severely limiting gas scrubbing, H_2SO_4 condensation and gas-rock
435 interaction. In summary, both sublimate mineralogy and Pb isotope composition of gas
436 support the idea of a recent hidden recharge of the shallow reservoir with hotter mafic
437 magmas. However, the inferred magma recharge and related temperature increase have not
438 been detected since the onset of thermal monitoring from space of the El Misti lava dome in
439 2000 (Moussallam et al., 2017), suggesting the recharge occurred before 2000. The recharge

perhaps could have been related to the last high fumarolic activity observed from Arequipa in 1984–1985 (Thouret et al., 2001).

Implications for hazards and volcanic monitoring

The activity of El Misti volcano is monitored from the height of the gas plume, edifice deformation, thermal emission, volcano-tectonic earthquakes, and the composition of geothermal waters. Collectively, the monitored parameters point to rather stable activity of the volcano at the decadal time scale. Moussallam et al. (2017) emphasized the need to also monitor major species of gas (H_2O, H_2, SO_2, H_2S), which allow for an estimation of gas-melt equilibrium temperature and oxygen fugacity. Here we suggest that the Pb isotopic composition of fumarolic minerals is less sensitive to short term change of degassing conditions and represents perhaps the most direct probe of recent magma composition. Monitoring the Pb isotope composition of El Misti gases would provide a window on the hidden cycles of magma recharge and differentiation, and would allow us to detect any departure from the steady-state regime that could potentially lead to an eruption.

Conclusions

We developed a new method to probe the hidden magmatic evolution of quiescent Andean volcanoes from the Pb isotope composition of gas emissions. The method is based on the properties of Pb isotopes that vary systematically during Assimilation - Fractional Crystallization (AFC) of magmas but do not fractionate during degassing. The method is applied to El Misti volcano that threatens the nearby city of Arequipa, the second most densely populated city of Peru.

Using this approach, we show that magmas currently degassing at El Misti volcano are on average more evolved than the centuries old lavas forming the conduit plug. This difference may reflect the secular differentiation of a single, large magma reservoir, or, alternatively, the contribution of a more evolved magma reservoir (possibly rhyolitic) to volcanic emanations. Conversely, the slight difference between the instantaneous composition recorded in gas condensate and the time-integrated composition recorded in solid deposits points to the degassing of less evolved magmas over the last decades. This trend indicates that El Misti

magma reservoir may be currently undergoing recharge by hotter more mafic magmas, consistent with the lack of Pb-rich sublimates and the predominance of low temperature minerals in fumarole deposits collected half a century ago. This work suggests that the Pb isotope composition of gas emissions is a promising tool for probing the hidden magmatic evolution of quiescent volcanoes where AFC is the dominant process.

Figure captions

Fig. 1 Location maps. (a) Map of South America showing the location of El Misti Volcano in the Central Volcanic Zone (CVZ). Northern (NVZ) and southern (SVZ) volcanic zones are indicated. (b) Satellite map of the El Misti area showing the location of Arequipa city. White line shows the approximate boundary of Arequipa suburbs in 2021. Source: Google, Images©2021 TerraMetrics. (3) Photo of El Misti lava plug inside the crater taken in October 2018. The locations and temperatures of the sampled fumaroles are indicated by arrows. The 120 m wide lava dome is located at the bottom of the 200 m deep inner crater.

Fig. 2 Images of the sublimates. (a-c) 150°C sublimates: (a) Binocular loupe photo of a grain covered with $PbCl_2$ and $PbSO_4$. (b) Scanning Electron Microscopy (SEM) image of the same grain. (c) SEM image of a grain with $CaSO_4$. (d-f) 260°C sublimates: (d) Macroscopic photo of $NaAl(SO_4)_2$ deposit. (e) and (f): SEM images showing PbS coating $NaAl(SO_4)_2$ foam. All SEM images were acquired at LMV using a JEOL JSM 5910LV microscope operating in Backscattered Electron (BSE) imaging mode.

Fig. 3 Trace element concentrations of El Misti fumarolic minerals and gas condensates. Data are shown for samples collected in 2018 (this work) and 1967 (Birnie and Hall, 1974). Trace elements are sorted from left to right according to their decreasing abundances in the 260°C condensate. Average concentrations are plotted for each sample type.

Fig. 4 $^{206}Pb/^{204}Pb$ plotted against the Pb fraction unsupported by silicate input. The silicate unsupported Pb fraction (i.e. the fraction of Pb originating from the gas) is equal to $1 - 1/EF_{Pb}$, where EF_{Pb} is the Pb enrichment factor (see text). Here, EF_{Pb} is calculated relative to titanium, assuming that all titanium in gas samples originates from rocks. The absence of correlation in this diagram argues against a control of rock particulates on the small Pb isotope variations.

Fig. 5 Plot of SiO_2 versus $^{206}Pb/^{204}Pb$ (a) and $^{208}Pb/^{206}Pb$ (b) for El Misti lavas younger than 11 ky (stage 4). This relation reflects the assimilation of unradiogenic Pb from the proterozoic Charcani gneiss (Arequipa Massif) during fractional crystallization of El Misti magmas. Samples include 6 ka old scoria bombs (MIS-00-20), two pumices from fall (quebrada San Lazaro) and

509 one dacitic pumice (MIS-02-10a) from the 2000 years B.P. eruption. Data are from Mamani et
510 al. (2008) (Pb isotopes) and Rivera et al. (2017) (SiO_2 content). Errors bars are for analytical
511 uncertainties. Best fit curves are shown. The single Pb data ($^{206}Pb/^{204}Pb$ of 17.38) reported for
512 El Misti rhyolites (Barreiro and Clark, 1984) suggests that rhyolites are not more contaminated
513 than dacites (vertical arrows), consistent with the final differentiation of rhyolites within El
514 Misti edifice (Tepley et al., 2013).
515
516 **Fig. 6** SiO_2 content of El Misti lavas and tephra plotted versus time. Data are from Thouret et
517 al. (2001), Rivera et al. (2017) and Tepley et al. (2013). The star and shaded rectangle show
518 the instantaneous and time-integrated SiO_2 contents of degassing magmas inferred from 2018
519 gas condensates and sublimates, respectively. (A) Single reservoir model (Ruprecht and
520 Wörner 2007). In this model, arrows indicate the inferred evolution of the magma reservoir
521 through time. Arrow 1 links the composition of the last erupted lavas (the conduit plug) with
522 the inferred composition of the currently degassing magma, pointing to a secular
523 differentiation trend. Arrow 2 links the time-integrated and instantaneous modelled SiO_2
524 contents. This trend suggests that the El Misti magma reservoir is currently undergoing
525 recharge by hot mafic magmas, in agreement with the evolution of fumaroles minerals during
526 the last half a century. (B) Two reservoir model (Tepley et al., 2013). In this model, emanations
527 from El Misti crater result from mixing gases escaping from the andesite and rhyolite
528 reservoirs (horizontal dashed arrows). In an end-member case, both reservoirs have more or
529 less constant compositions through time (vertical arrows), and the composition of gases
530 reflects varying contributions of the two magma reservoirs. In this model, the contribution of
531 the rhyolite reservoir to the Pb gas flux is estimated at 38% over the last decades, and 27%
532 currently (see text).

533 **References**

534

535 Africano F, Van Rompaey G, Bernard A, Le Guern F (2002) Deposition of trace elements from
536 high temperature gases of Satsuma-Iwojima volcano. Earth Planets Space 54: 275-286.
537 Barreiro BA, Clark AH (1984) Lead isotopic evidence for evolutionary changes in magma-crust
538 interaction, Central Andes, southern Peru. Earth Planet Sci Lett 69: 30-42.
539 Birnie RW, Hall JH (1974) The geochemistry of El Misti volcano, Peru fumaroles. Bull Volcanol
540 38, 1.
541 Brearley M, Scarfe C (1986) Dissolution Rates of Upper Mantle Minerals in an Alkali Basalt
542 Melt at High Pressure: An Experimental Study and Implications for Ultramafic Xenolith
543 Survival. J Petrol 27: 1157-1182.
544 Bullard F (1962) Volcanoes of southern Peru. Bull Volc 24: 443–453.
545 Cobeñas G, Thouret J-C, Bonadonna C, Boivin P (2012) The c. 2030 yr BP Plinian eruption of El
546 Misti volcano, Peru: eruption dynamics and hazard implications. J Volcanol Geotherm
547 Res 241 – 242: 105–120.
548 Chavéz Chavéz JA (1992) La erupción del volcán Misti, pasado, presente, futuro: Arequipa.
549 Impresiones Zenit, Arequipa-Peru (158 p).
550 Deniel C, Pin C (2001) Single-stage method for the simultaneous isolation of lead and
551 strontium from silicate samples for isotopic measurements. Anal Chim Acta 426: 95–
552 103.
553 De Paolo D.J. (1981) Trace Element and Isotopic Effects of Combined Wallrock Assimilation
554 and Fractional Crystallization. Earth Planet Sci Lett 53: 189-202. DOI : 10.1016/0012-
555 821X(81)90153-9.
556 Gauthier P-J, Le Cloarec M-F, Condomines M (2000) Degassing processes at Stromboli volcano
557 inferred from short-lived disequilibria (^{210}Pb-^{210}Bi-^{210}Po) in volcanic gases. J Volcanol
558 Geotherm Res 102: 1-19.
559 Hantke G, Parodi A (1966) Catalogue of the active volcanoes of the world. Part XIX: Colombia,
560 Ecuador and Peru: Naples, IAVCEI, 73 p.
561 Harpel C, de Silva S, Salas G (2011) The 2 ka Eruption of Misti Volcano, Southern Peru—The
562 Most Recent Plinian Eruption of Arequipa's Iconic Volcano. Geol Soc Am Spec papers
563 Vol. 484 (72 pp.).

564 INEI (2018). Directorio Nacional de Centros Poblados, Censo Nacional 2017: XII de Población,
565 VII de Vivienda y III de Comunidades Indígenas
566 (https://www.inei.gob.pe/media/MenuRecursivo/publicaciones_digitales/Est/Lib1541
567 /index.htm)
568 Johnson ML, Burnett DS (1993) SO2–rock interaction on Io: Reaction under highly oxidizing
569 conditions. J Geophys Res 98: 1223–1230.
570 Kiebala A (2008) Magmatic Processes by U-Th Disequilibria Method. Comparison of Two
571 Andean Systems: El Misti Volcano (S. Peru) and Taapaca Volcanic Center (N. Chile). (PhD.
572 Thesis). Georg-August-Universität Göttingen, Germany (93 pp.).
573 Mamani M, Tassara A, Wörner G (2008), Composition and structural control of crustal
574 domains in the central Andes, Geochem Geophys Geosyst 9, Q03006,
575 doi:10.1029/2007GC001925.
576 Moussallam Y, Peters N, Masias P, Apaza F, Barnie T, Schipper CI, Curtis A, Tamburello G,
577 Aiuppa A, Bani P, Giudice G, Pieri D, Davies AG, Oppenheimer C (2017). Magmatic gas
578 percolation through the old lava dome of El Misti volcano. Bull Volcanol 79:46. DOI:
579 10.1007/s00445-017-1129-5.
580 Richter FM (2004) Timescales determining the degree of kinetic isotope fractionation by
581 evaporation and condensation. Geochim Cosmochim Acta 68: 4971–4992.
582 Rivera M, Martin H, Le Pennec J-L, Thouret J-C, Gourgaud A, Gerbe M-C (2017) Petro-
583 geochemical constraints on the source and evolution of magmas at El Misti volcano
584 (Peru). Lithos 268–271: 240–259. DOI: 10.1016/j.lithos.2016.11.009.
585 Ruprecht P, Wörner G. (2007) Variable regimes in magma systems documented in plagioclase
586 zoning patterns: El Misti strato-volcano and Andahua monogenetic cones. J Volcanol
587 Geotherm Res 165: 142–162. DOI: 10.1016/j.jvolgeores.2007.06.002.
588 Sainlot N, Vlastelic I, Nauret F, Moune S, Aguilera F (2020a) Sr-Pb isotopes signature of Lascar
589 volcano (Chile): Insight into contamination of arc magmas ascending through a thick
590 continental crust. J South Am Earth Sci 101: 102599, DOI:
591 10.1016/j.jsames.2020.102599, 2020.
592 Sainlot N, Vlastelic I, Moune S, Rose-Koga EF, Schiavi F, Valade S, Aguilera F (2020b) Uptake of
593 gaseous thallium, tellurium and vanadium into anhydrous alum, Lascar volcano
594 fumaroles, Chile. Geochim Cosmochim Acta 275: 64-82.

595 Symonds RB, Rose WI, Reed MH, Lichte FE, Finnegan DL (1987) Volatilization, transport and
596 sublimation of metallic and non-metallic elements in high temperature gases at Merapi
597 Volcano, Indonesia. Geochim Cosmochim Acta 51: 2083–2101.
598 Taran YA, Bernard A, Gavilanes JC, Africano F (2000) Native gold in mineral precipitates from
599 high-temperature volcanic gases of Colima volcano, Mexico. Appl Geochem 15: 337–
600 346.
601 Tepley FJ, de Silva S, Salas G (2013) Magma dynamics and petrological evolution leading to the
602 VEI 5 2000 BP eruption of El Misti volcano, southern Peru. J Petrol 54: 2033–2065. DOI:
603 10.1093/petrology/egt040.
604 Tilton GR, Barreiro BA (1980) Origin of lead in Andean calcalkaline lavas, southern Peru,
605 Science 210, 1245-1247.
606 Thompson AB, Matile L, Ulmer P (2002) Some Thermal Constraints on Crustal Assimilation
607 during Fractionation of Hydrous, Mantle-derived Magmas with Examples from Central
608 Alpine Batholiths, J Petrol 43, 403–422. DOI: 10.1093/petrology/43.3.403.
609 Thouret, J-C, Finizola A, Fornari M, Suni J, Legeley-Padovani A, Frechen M (2001) Geology of
610 El Misti volcano nearby the city of Arequipa, Peru. Geol Soc Am Bull 113: 1593–1610.
611 Todt W, Cliff RA, Hanser A, Hofmann AW (1996) Evaluation of a ^{202}Pb–^{205}Pb double spike for
612 high-precision lead isotope analysis, in Earth Processes. In Reading the Isotopic Code
613 (eds. A. Basu and S. Hart). AGU, pp. 429–437.
614 Vlastélic I, Staudacher T, Deniel C, Devidal JL, Devouard B, Finizola A, Télouk P (2013) Lead
615 isotopes behavior in the fumarolic environment of the Piton de la Fournaise volcano
616 (Réunion Island). Geochim Cosmochim Acta 100: 297-314. DOI:
617 10.1016/j.gca.2012.09.016.
618 Wörner G, Moorbath S, Harmon RS (1992) Andean cenozoic volcanics reflect basement
619 isotopic domains. Geology 20: 1103-1106.
620 Zelenski M, Simakin A, Taran Y, Kamenetsky VS, Malik N (2021) Partitioning of elements
621 between high-temperature, low-density aqueous fluid and silicate melt as derived from
622 volcanic gas geochemistry. Geochim Cosmochim Acta 295: 112:134. DOI:
623 10.1016/j.gca.2020.12.011.

F1

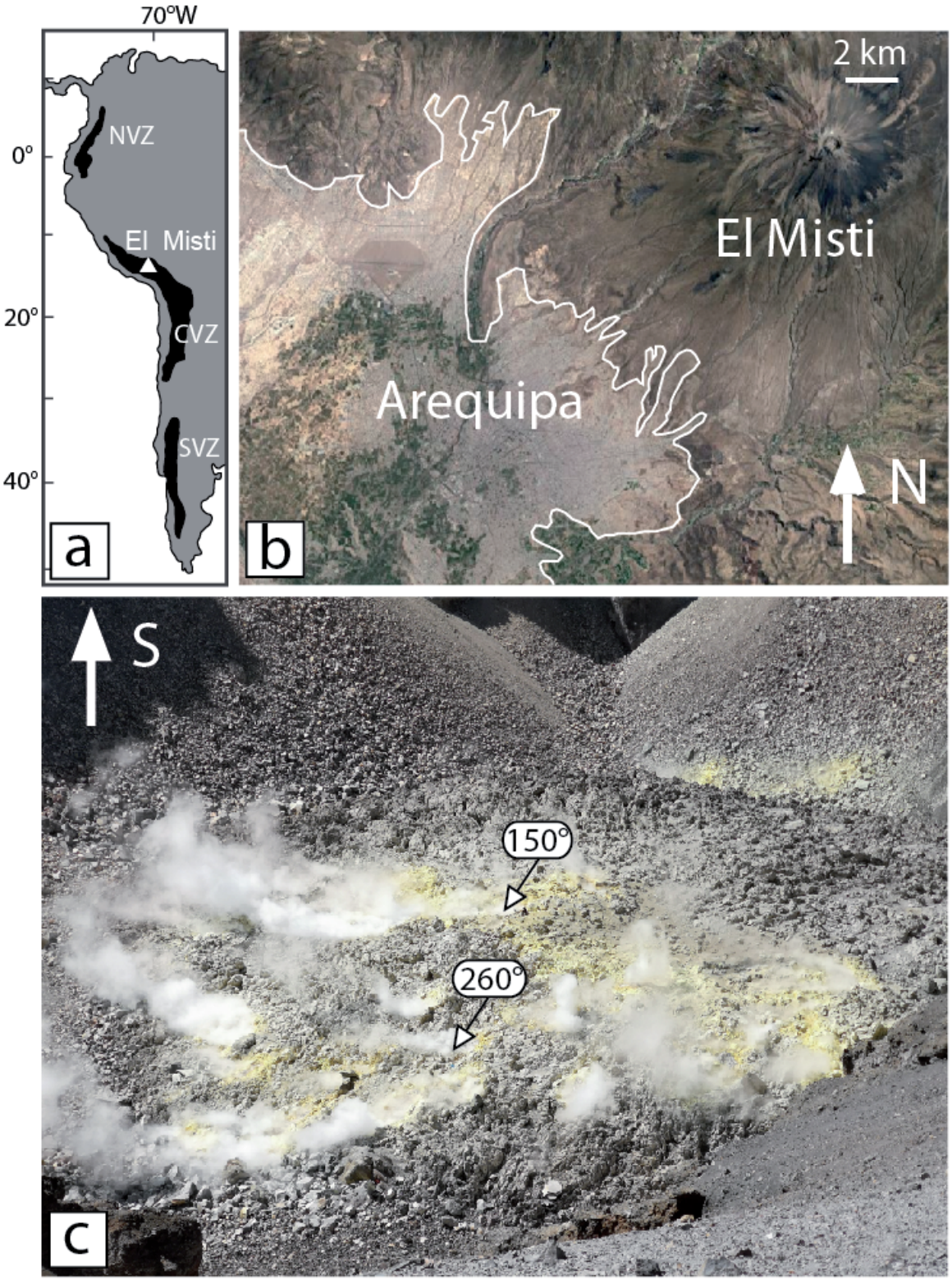
70°W
0°
20°
40°
NVZ
El Misti
CVZ
SVZ
a
2 km
El Misti
Arequipa
N
b
S
150°
260°
c

F2

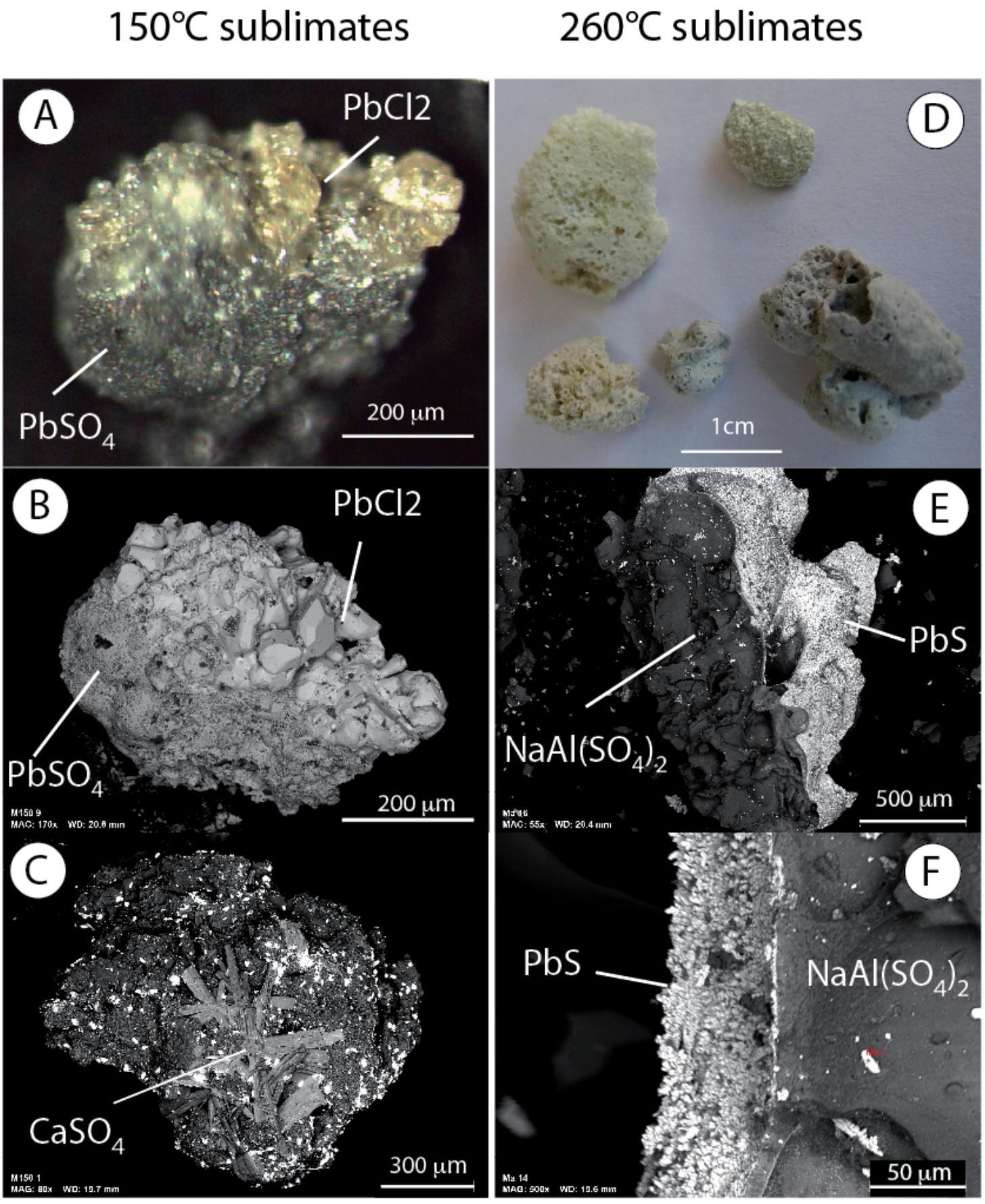
150°C sublimates
260°C sublimates
A
PbCl2
PbSO4
200 µm
D
1cm
B
PbCl2
PbSO4
200 µm
E
PbS
NaAl(SO4)2
500 µm
C
CaSO4
300 µm
F
PbS
NaAl(SO4)2
50 µm

F3

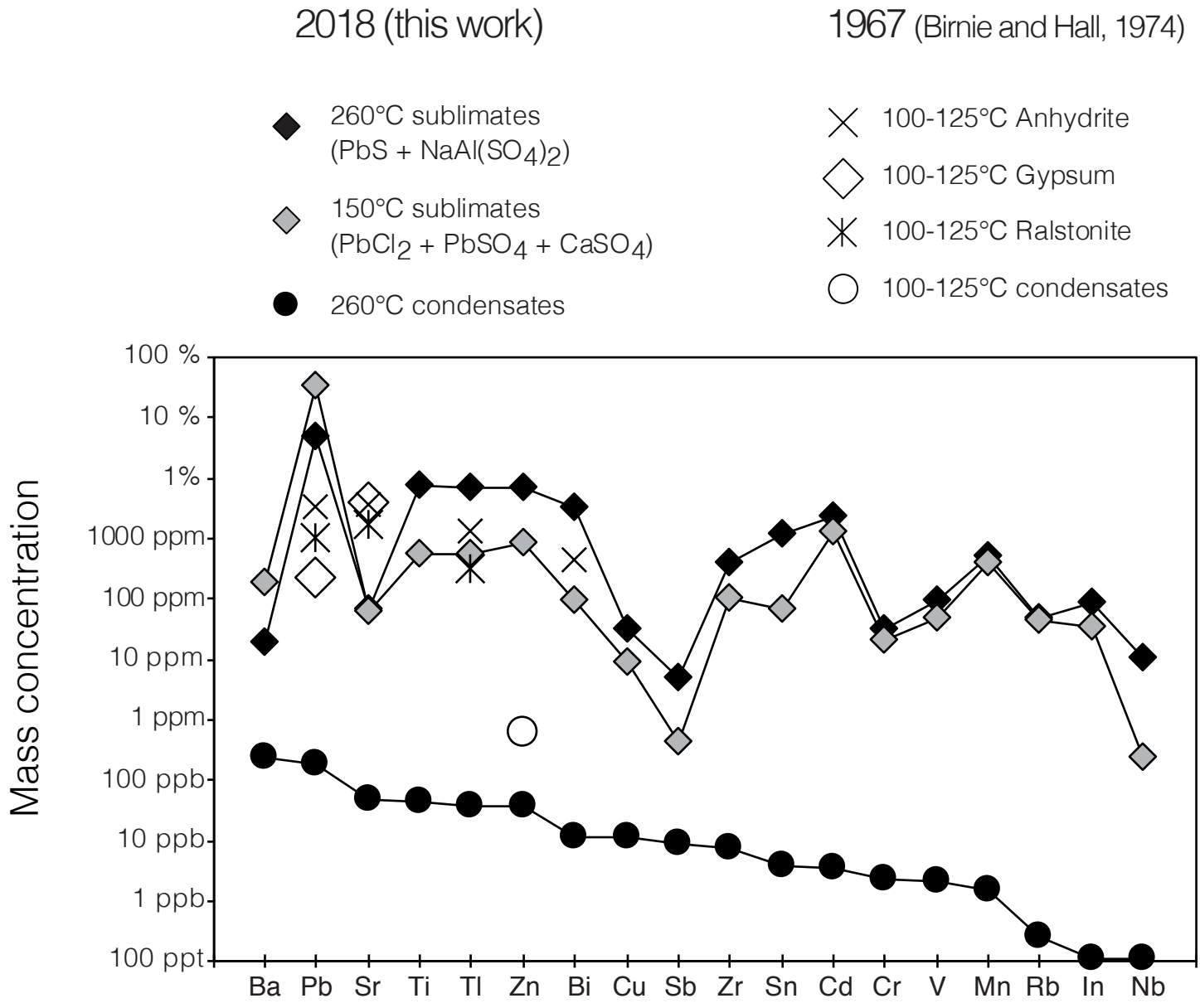
2018 (this work)
1967 (Birnie and Hall, 1974)
260°C sublimates
(PbS + NaAl(SO4)2)
150°C sublimates
(PbCl2 + PbSO4 + CaSO4)
260°C condensates
100-125°C Anhydrite
100-125°C Gypsum
100-125°C Ralstonite
100-125°C condensates
Mass concentration
100 %
10 %
1%
1000 ppm
100 ppm
10 ppm
1 ppm
100 ppb
10 ppb
1 ppb
100 ppt
Ba Pb Sr Ti Tl Zn Bi Cu Sb Zr Sn Cd Cr V Mn Rb In Nb

F4

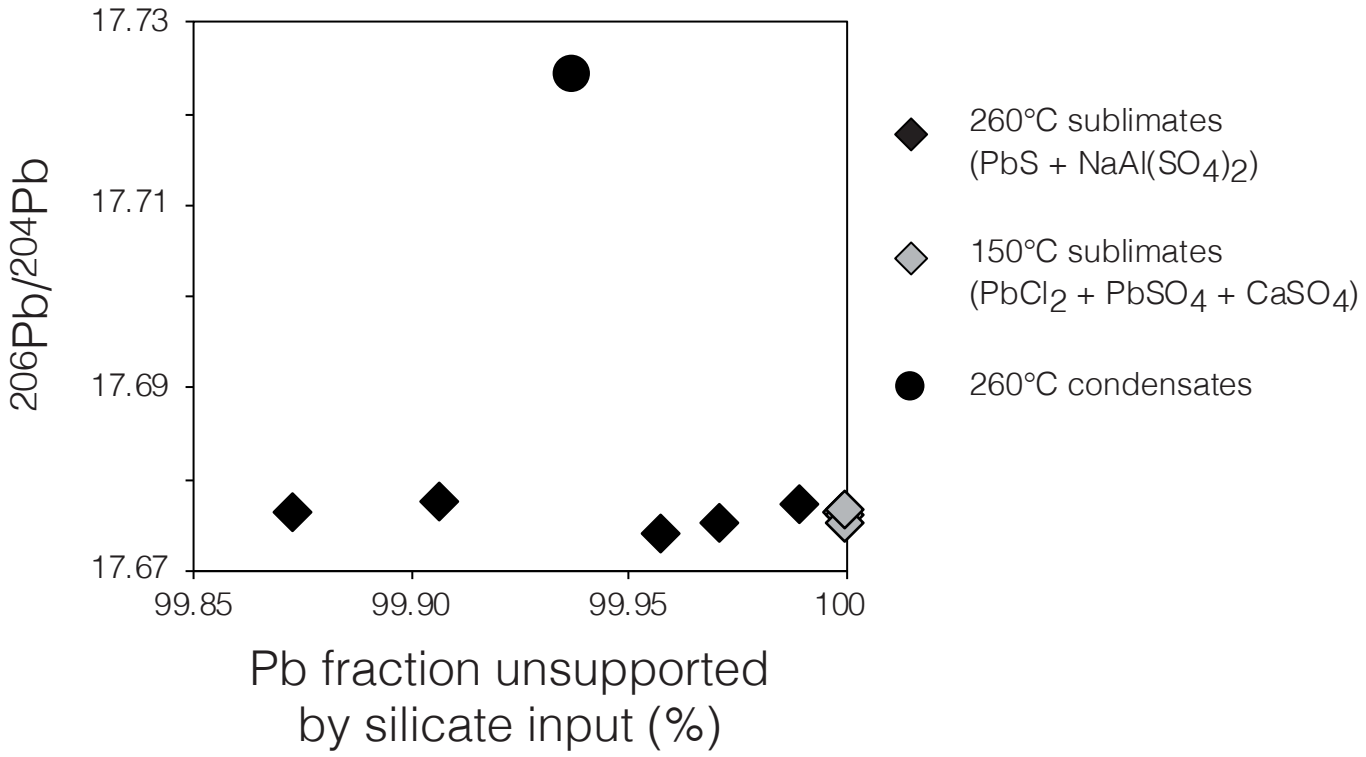
17.73
17.71
17.69
17.67
206Pb/204Pb
99.85
99.90
99.95
100
Pb fraction unsupported
by silicate input (%)
260°C sublimates
(PbS + NaAl(SO4)2)
150°C sublimates
(PbCl2 + PbSO4 + CaSO4)
260°C condensates

AFC Misti 4

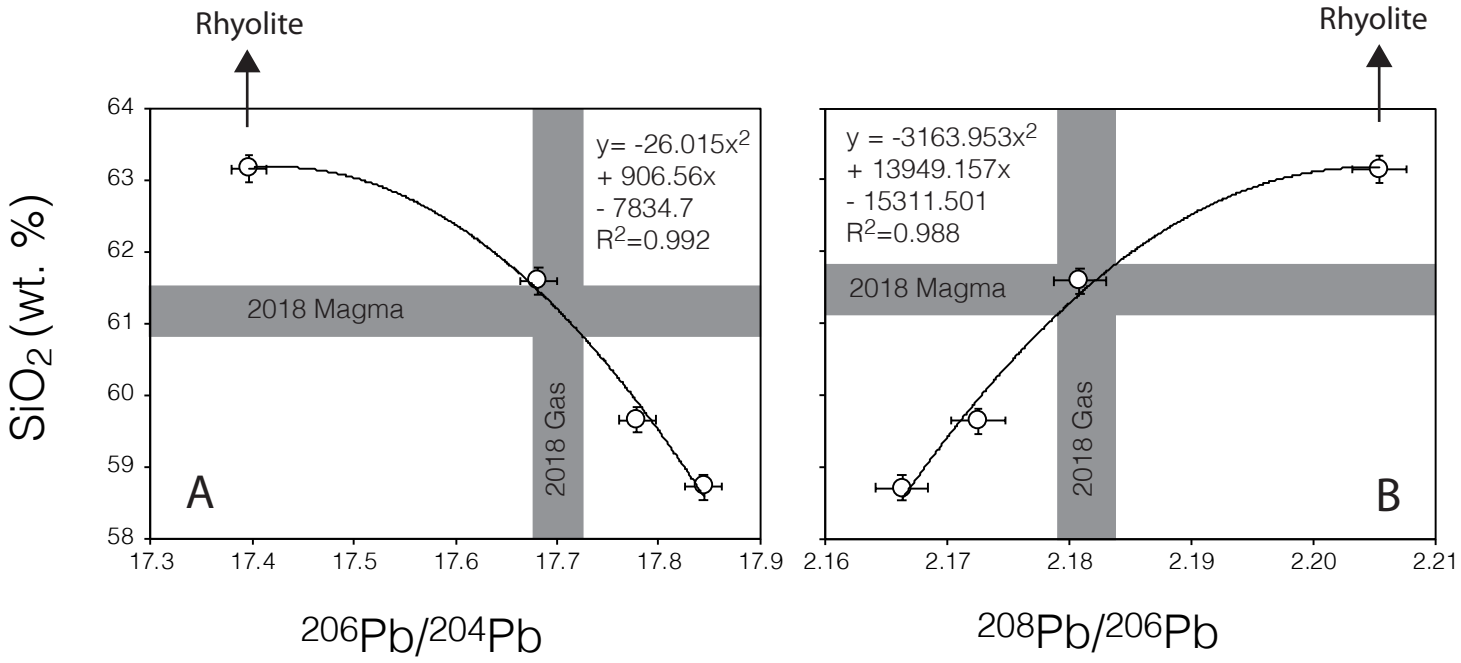
Rhyolite
Rhyolite
SiO2 (wt. %)
64
63
62
61
60
59
58
y= -26.015x2
+ 906.56x
- 7834.7
R2=0.992
2018 Magma
2018 Gas
A
17.3
17.4
17.5
17.6
17.7
17.8
17.9
206Pb/204Pb
y = -3163.953x2
+ 13949.157x
- 15311.501
R2=0.988
2018 Magma
2018 Gas
B
2.16
2.17
2.18
2.19
2.20
2.21
208Pb/206Pb

F6

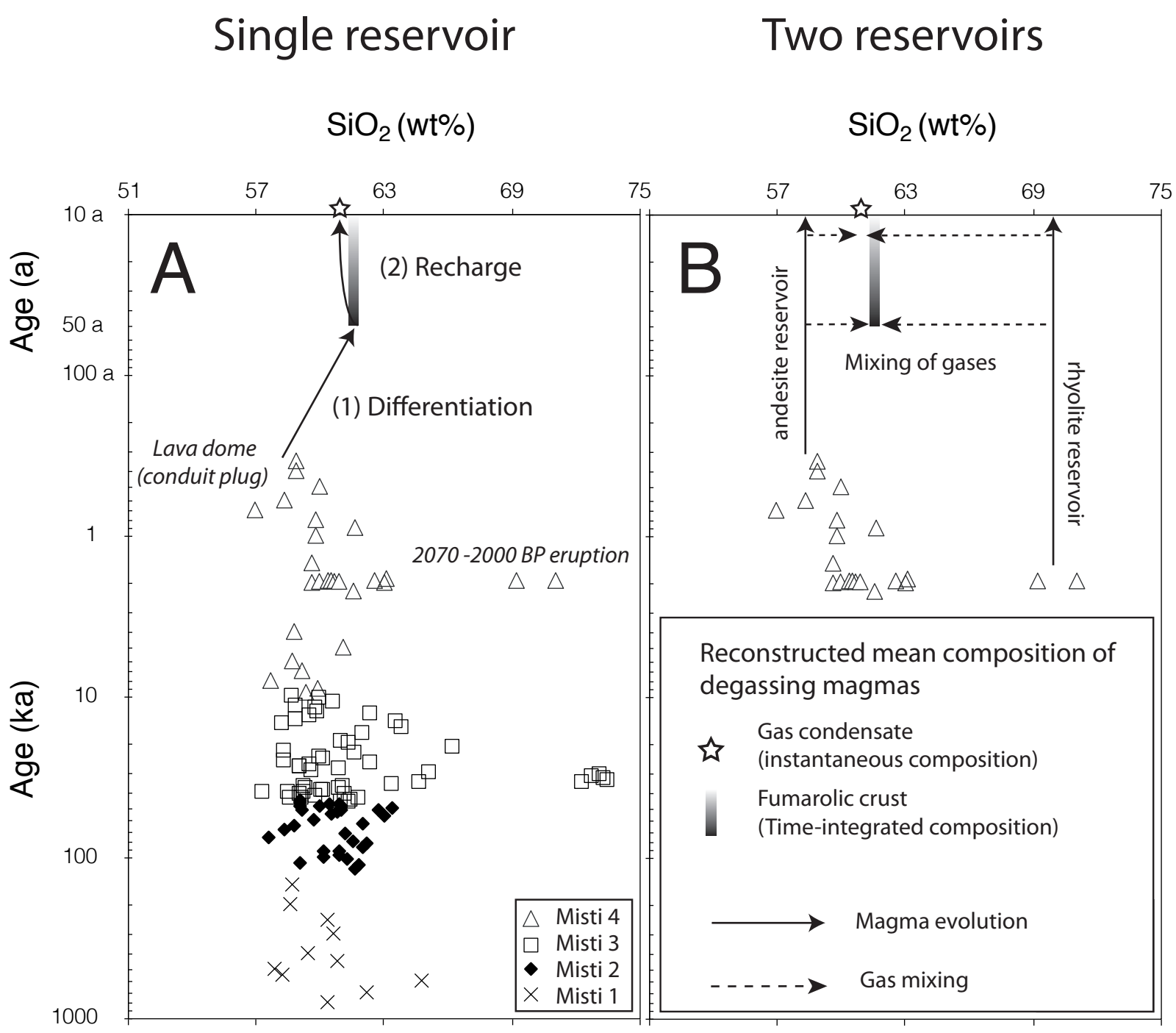
Single reservoir
Two reservoirs
SiO2 (wt%)
SiO2 (wt%)
51
57
63
69
75
57
63
69
75
10 a
50 a
100 a
1
10
100
1000
Age (a)
Age (ka)
A
B
(2) Recharge
(1) Differentiation
Lava dome
(conduit plug)
2070 -2000 BP eruption
andesite reservoir
rhyolite reservoir
Mixing of gases
Misti 4
Misti 3
Misti 2
Misti 1
Reconstructed mean composition of degassing magmas
Gas condensate
(instantaneous composition)
Fumarolic crust
(Time-integrated composition)
Magma evolution
Gas mixing

Table 1: Chemical and isotopic composition of 2018 El Misti condensates and sublimates

Sample type	Gas condensate	Gas sublimates					Gas sublimates			
Temperature	260°C	260°C					150°C			
Mineralogy		PbS + NaAl(SO4)2					PbCl2 + PbSO4 + CaSO4			
		#a	#b	#c	#d	#e	#1	#3	#4	#5
	ppb	wt%	wt%	wt%	wt%	wt%	wt%	wt%	wt%	wt%
Pb	177	3.80	4.90	2.01	2.82	9.86	16.8	36.3	32.4	44.5
	ppb	ppm	ppm	ppm	ppm	ppm	ppm	ppm	ppm	ppm
Ti	45.0	6593	5734	10338	10649	4228	822	410	522	405
V	2.04	96	90	105	104	64	73	49	50	24
Cr	2.27	33	30	39	38	22	40	15	19	7
Mn	1.52	589	559	454	465	578	344	646	500	112
Cu	11.4	51	44	26	25	18	5	12	10	10
Zn	37.0	5393	6094	6842	7008	9363	1689	645	589	399
Rb	0.25	63	66	42	42	36	38	43	78	12
Sr	45.7	36	37	10	9	234	10	108	51	84
Zr	7.65	233	195	605	601	305	134	121	96	46
Nb	0.11	19	17	6	6	4	0	0	0	0
Cd	3.35	2141	2277	2158	2158	3306	2257	1304	1016	539
In	0.11	45	55	70	74	173	77	29	23	13
Sn	3.87	896	814	637	606	3160	138	51	51	35
Sb	8.74	9	9	2	2	3	0.2	0.6	0.4	0.6
Ba	244	34	33	6	6	18	39	26	411	260
Tl	38.3	5283	9479	7731	7868	4097	1349	234	142	514
Bi	11.7	2314	2210	3182	3441	4617	81	115	82	113
206Pb/204Pb	17.7253	17.6743	17.6751	17.6764	17.6776	17.6778	17.6764	17.6762	17.6753	17.6765
duplicate	17.7234 r	17.6738 d				17.6770 d				
207Pb/204Pb	15.5935	15.5843	15.5851	15.5853	15.5866	15.5866	15.5824	15.5820	15.5818	15.5823
duplicate	15.5910 r	15.5838 d				15.5858 d				
208Pb/204Pb	38.6298	38.5999	38.6033	38.6048	38.6073	38.6076	38.5929	38.5906	38.5898	38.5923
duplicate	38.6264 r	38.5985 d				38.6049 d				

Pb isotope ratios are relative to the NBS 981 values of Todt el al. (1996)

r: duplicate run

d: duplicate chemistry